Liquid-Liquid Phase Separation of the Green Mussel Adhesive Protein Pvfp-5 is Regulated by the Post-Translated Dopa Amino Acid

Kanagavel Deepankumar[1,#], Qi Guo[1,#], Harini Mohanram[2], Jessica Lim[2], Yuguang Mu[2], Konstantin Pervushin[2], Jing Yu[1,] and Ali Miserez[1,2,*]*

[1] Center for Sustainable Materials (SusMat), School of Materials Science and Engineering, Nanyang Technological University (NTU), 50 Nanyang Avenue, 637,553, Singapore

[2] School of Biological Sciences, NTU, 60 Nanyang Drive, 637,551, Singapore

[#] These authors contributed equally to the study

[*] Authors for correspondence: ali.miserez@ntu.edu.sg; yujing@ntu.edu.sg

Abstract

The underwater adhesive prowess of aquatic mussels has been largely attributed to the presence of the post-translationally modified amino acid 3,4-dihydroxylphenylalanine (Dopa) in mussel foot proteins (MFPs) that make up their adhesive threads. In parallel, it has been suggested that during thread fabrication, MFPs form intermediate fluidic phases such as liquid crystals or coacervates during a Liquid-Liquid Phase Separation (LLPS) process. Here, we show that Dopa plays another central role during mussel fiber formation, by enabling LLPS of Pvfp-5β, a main MFP of the Asian green mussel *Perna viridis*. Using residue-specific substitution of Tyrosine (Tyr) for Dopa during recombinant expression, we show that Dopa-substituted Pvfp-5β exhibits LLPS under seawater-like conditions, whereas the Tyr-only version forms insoluble aggregates. Combining quantum chemistry calculations and solution NMR studies, we find that a transient H-bonding network requiring the two hydroxyl groups of Dopa is critical to enable LLPS in Dopa-mutated Pvfp-5β. Overall, our study suggests that Dopa plays an important role in regulating LLPS of MFPs, which may be critical to concentrate the adhesive proteins at the plaque/substrate interface and therefore produce a more robust adhesive. Our findings also provide molecular-level lessons to guide biomanufacturing of protein-based materials such as bioadhesives and load-bearing fibers.

Keywords: Mussel foot proteins, Dopa, liquid-liquid phase separation, NMR, quantum chemistry calculations.

1. Introduction

The water-resistant adhesive ability of aquatic mussels has been mainly attributed to the high content of the post-translated amino acid Di-Hydroxyphenylalanine (Dopa) in mussel foot proteins (MFPs)[1-2], the building blocks of mussel adhesive threads, called the byssus[3-4]. The catecholic Dopa side-chain indeed exhibits versatile physico-chemical features that makes it well-suited to adsorb and adhere to immersed substrates, including the ability to engage into numerous types of intermolecular interactions such as coordination bonding[2, 5], hydrogen bonding[6], and hydrophobic interactions[7].

While there has been undeniable success in synthesizing catechol-containing polymers for enhanced water-resistant adhesives and coatings[8-9], recent investigations have indicated that this Dopa "paradigm" of mussel adhesion may be subtler than previously proposed. Notably, both nano-scale and macroscopic adhesion studies of recombinant MFPs and MFP-derived peptides from the adhesive plaque – the section of the byssus in direct contact with substrates – have indicated that comparable levels of adhesion can be achieved even when tyrosine residues (Tyr) are not post-translated into Dopa. In particular for the Asian green mussel (*Perna viridis*), Bilotto[10] *et al*. reported Surface Force Apparatus (SFA) adhesion measurements of the foot protein 5 (Pvfp-5β)[11] containing either Tyr or with most Tyr substituted to Dopa, and did not find statistically-significant differences of adhesion strengths and energies between the two variants. Likewise, Ou[12] *et al.* – also using Pvfp-5β as a model mussel adhesive protein – measured equivalent macroscopic adhesive strength values for Pvfp-5β when Tyr was enzymatically modified to Dopa. These results can be reconciled by the study of Maier[13] *et al*. together with Molecular Dynamic (MD) simulations by Ou *et al.*[12] The former reported that hydrated ions on oxide surfaces are evicted by Lys residues, enabling adjacent Dopa residues to form bidentate H-bonding with the oxide surface unimpeded by these hydrated ions, whereas the latter predicted that the

reverse stepwise process, namely initial eviction of surface ions by aromatic residues followed by electrostatic binding of positively-charged residues, was also possible. Importantly, MD simulations revealed that Tyr is equally efficient at sweeping the surface of hydrated ions, thus eliminating their screening effect and enabling adjacent Lys residues to bind to the surface *via* electrostatic interactions. In addition, nanoscale adhesion studies on MFP-mimetic peptides[14] have shown that the sole presence of aromatic side-chains, free of single or double hydroxyl groups of Tyr and Dopa, respectively, was sufficient to promote strong adhesion through π-cation interactions. In fact, among mussel-mimetic peptides with identical sequences and containing either Dopa, Tyr, or phenylalanine (Phe) as aromatic residues, the latter exhibited the highest reversible adhesion interactions[14]. Similar to these trends, our team recently reported the adhesive properties of a β-sheet-rich structural protein (suckerin-12) comprising either Tyr or Dopa along its primary sequence[15]. Both versions were characterized by evenly high adhesion energies.

Concurrently to these studies, there has been increasing evidence that the natural biofabrication of byssal threads is enabled by the formation of intermediate, fluid-like phases within which MFPs are highly concentrated by a liquid-liquid phase separation (LLPS) process. Notably, we have reported visual observations of a liquid-like secretion along the groove of the foot during byssal thread formation[16-18] as illustrated in time-resolved images of thread formation in Figures 1a-b. In separate studies, Harrington and co-workers[19] have demonstrated that MFPs of *Mytilid* species are compartmentalized as 1-2 µm vesicles in large secretory glands and suggested that MFPs forming the adhesive plaques are stored as dense fluid phases, possibly coacervate microdroplets and/or liquid crystals. In the same vein, evidence that MFPs self-assemble into fluid coacervates as an intermediate phase towards adhesive plaque maturation was also demonstrated by Valois *et al*.[20] who established that the coacervate microdroplet environment shields Dopa residues from

premature oxidation. Delay of Dopa oxidation in the plaque-forming gland where MFPs are stored prior to adhesive plaque secretion has also been corroborated by Priemel[21] *et al*. Finally, the critical involvement of LLPS in adhesive plaque formation is also supported by the earlier study of Wei[22] *et al.* who established that purified MFP-3-*slow*, an adhesive and matrix protein of the adhesive plaque in *Mytulis* genus, can form coacervate microdroplets *in vitro*.

Therefore, since Dopa-rich MFPs of adhesive plaques have been evidenced to form coacervates and since adhesive glands also contain vesicle with coacervates-like characteristics, in this study we asked the question whether Dopa may play a role in the LLPS ability of MFPs? To address this hypothesis, we selected the adhesive foot protein Pvfp-5β from the Asian green mussel (*Perna viridis*) and exploited our ability to directly incorporate Dopa during recombinant protein expression using an auxotrophic *E. coli* strain that enables the residue-specific substitution of Tyr for Dopa[23-24]. In what follows, the Tyr- and Dopa-containing variants of Pvfp-5β are named Pvfp-5-Tyr and Pvfp-5-Dopa, respectively. In *Perna viridis*, adhesive foot proteins are secreted in a time-regulated fashion during adhesive thread fabrication[16], with Pvfp-5β the frontline protein in this process. Similar to MFP-3 from Mytilid species, Pvfp-5β contains multiple pairs of Dopa (or Tyr)-cationic residues that have been proposed to promote adhesion by evicting hydrated cations from the surface as explained above[13]. Native Pvfp-5β was also demonstrated to displace surface water by Attenuated Total Reflection Infrared Spectroscopy (ATR-FTIR), thus enhancing adsorption and adhesion[16]. Because of its homology to a tandem repeat of an Epidermal Growth Factor (EGF) motif, Pvfp-5β has been predicted to exhibit an elongated, yet flexible conformation with a few β-strands[16], which was corroborated by Circular Dichroism (CD) as well as solution NMR studies[25]. Another structural feature that is relevant in the context of this study is that Tyr and Dopa are predicted to be exposed to solvent[16].

For both Pvfp-5β variants, we systematically investigated their phase behavior under a broad range of pH and ionic strength conditions. We find that Dopa substitution leads to LLPS near physiological conditions, whereas the Tyr version does not, and instead aggregates above neutral pH. On the basis of solution NMR studies of both proteins combined with quantum chemistry (QC) computations of inter-residue interactions of aromatic Tyr or Dopa side-chains, we find that LLPS in Pvfp-5-Dopa is enabled by the formation of a transient triangular hydrogen bonding (H-bonding) network that can only occur when two hydroxyl groups (Dopa) are present on the aromatic ring, as well as by Dopa-Dopa (π-π) stacking. In contrast, stronger π-cation attractive interactions are most favorable in the Tyr version, indicating that the resident time and strength of attractive interactions (dubbed as "stickers" in LLPS) in coacervate microdroplets is a key criterion governing phase separation behavior.

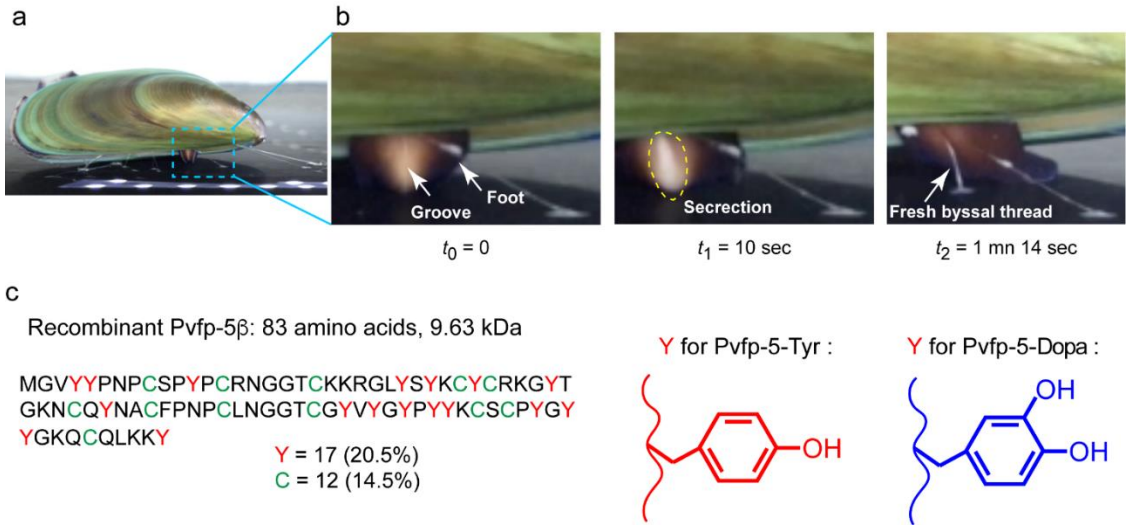

Figure 1. Time-step formation of a byssal thread of an Asian green mussel (*Perna virids*). **(a)** Overall view of a mussel with the foot (boxed in blue in the lower-right corner) in contact with the surface, ready to start secretion of a thread. **(b)** Enlarged views of the mussel foot at different time points during thread fabrication. The thread is secreted within the ventral groove of the foot. At t_0 (left), the mussel has committed to the surface and the foot starts to secrete the thread. At t_1 (middle) a whitish fluid secretion can be seen along the groove. At t_2 (right), the foot is retracting and a freshly formed thread can be seen. All still images captured from Supplementary Video 2 of *Ref*. [[16] (Copyright Creative Commons Attribution 4.0). **(c)** Sequence of recombinant Pvfp-5β. Y is either Tyr or Dopa for Pvfp-5-Tyr and Pvfp-5-Dopa, respectively.

2. Results and Discussion

2.1 Production and characterization of Pvfp-5-Tyr and Dopa-incorporated Pvfp-5-Dopa

Pvfp-5 contains seventeen Tyr residues that were intended to be replaced with the non-canonical Dopa through the *in vivo* residue specific incorporation (Figure 1c). Pvfp-5-Tyr and Pvfp-5-Dopa were predominantly expressed in the inclusion bodies. The purity of the Pvfp-5 variants was assessed by SDS-PAGE gel and estimated to be above 95% (Figure S1a, Supporting Information). To verify that Dopa was successfully incorporated into Pvfp-5β, we first employed a nitroblue tetrazolium (NBT) redox-staining assay, which detects redox-active residues in proteins such as Dopa. Pvfp-5-Dopa was NBT-positive on the SDS-PAGE gel, whereas Pvfp-5-Tyr was NBT-negative (Figure S1b, Supporting Information). Amino acid chromatograms and Matrix Assisted Laser Desorption-Time of Flight mass spectrometry (Maldi-ToF) further confirmed the depletion of Tyr and its replacement with Dopa in Pvfp-5-Dopa. The molecular weights obtained by Maldi-ToF for Pvfp-5-Tyr and Pvfp-5-Dopa were 9,657 Da and 9,935 Da, respectively (Figure S2, Supporting Information). Amino acid composition analyses of purified Pvfp-5 variants closely matched the predicted composition of the Pvfp-5 primary sequences (Figure S3, Table S1 and S2, Supporting Information). Dopa incorporation yield in Pvfp-5-Dopa was *ca*. 98% based on Maldi-ToF spectra and amino acid analysis, which is greater than the enzymatic conversion of Dopa using mushroom tyrosinase[12]. Circular dichroism (CD) spectra were used to assess the secondary structure of Pvfp-5-Tyr and Pvfp-5-Dopa in 10 mM acetic acid solution. At 5 $mg \cdot mL^{-1}$, the spectra exhibited random-coil structure with a minimum in the 195–200 nm range (Figure S4, Supporting Information). Compared to Pvfp-5-Tyr, Pvfp-5-Dopa displayed a negative shoulder peak around 225 nm that can be attributed to the Dopa side-chain, as recently reported for Dopa-rich short peptides[26], and the main negative peak of Pvfp-5-Dopa was also slightly shifted to a higher wavelength of the disordered region. Therefore,

introducing Dopa instead of Tyr appears to only slightly influence the secondary structure of Pvfp-5β.

One dimensional ^{1}H NMR spectra of Pvfp-5-Tyr and Pvfp-5-DOPA proteins were also acquired. The absence of peaks below 9.5 ppm and above 0 ppm confirmed that both proteins were largely unstructured (Figure S5a, Supporting Information). 2D ^{1}H-^{15}N HSQC spectra of Pvfp-5-Tyr displayed sharp peaks but over a narrow range (8.3 - 7.6 ppm), also pointing out towards a disordered conformation (Figure S5b, Supporting Information). The amide (NH-NH) diagonal region of the 2D ^{1}H-^{1}H TOCSY and ^{1}H-^{1}H NOESY spectra were then compared (Figure S5c, green and blue spectra respectively). We noted small intensity NOEs in NOESY spectra (black arrow, Figure S5c, Supporting Information) in addition to cross peaks of the protons from TOCSY, suggesting the presence of some localized structural features, most likely β-strands previously predicted to belong to EGF-domains (Figure S5c, Supporting Information)[16]. These cross peaks were found to be absent in 2D ^{1}H-^{1}H TOCSY spectra.

2.2 Adhesion properties of Pvfp-5 variants

To investigate the effect of Dopa resides in the adhesion of Pvfp-5β, we used the Surface Force Apparatus (SFA)[27] technique to compare the adhesive properties of Pvfp-5-Dopa and Pvfp-5-Tyr. For each protein, 20 μL of 20 μg/ml protein solution was injected in between two mica surfaces and left to adsorb on the surfaces for 30 min before the force measurements. The interaction of the two protein-adsorbed mica surfaces was measured as a function of separation distance (*D*) between two surfaces (Figures 2a-b) in a symmetric geometry. Upon separation, a sudden jump out of two surfaces can be measured if there is a strong adhesive interaction between the protein and mica surfaces[27-29]. The adhesion force measured can then be converted to the adhesion energy between two flat surfaces by using the JKR approximation:

$$E_{\mathrm{ad}} = 2F_{\mathrm{ad}}/3\pi R \quad (1)$$

Pvfp-5-Dopa and Pvfp-5-Tyr showed very similar adhesive properties in solution. The adhesion energies measured in acetic buffer (pH = 3.6) were -5.97 ± 0.25 and -8.26 ± 0.26 mJ/m^2 for Pvfp-5-Dopa and Pvfp-5-Tyr, respectively. The adhesion energies decreased to -1.27 ± 0.05 for Pvfp-5-Dopa and -1.75 ± 0.06 mJ/m^2 for Pvfp-5-Tyr upon increasing the pH of the solution to 7.4, which was achieved by replacing the acetic buffer with phosphate buffer. Additionally, the thickness of the protein layer, indicated by the hard-wall thickness of the SFA force-distance profile, increased from ~ 3 – 6 nm to ~ 10 – 15 nm upon increasing the pH of the solution, indicating that Pvfp-5 aggregated at pH 7.4. The decrease of the adhesion force of both proteins at neutral pH suggests that the adhesion force measured is largely of electrostatic origin. Since the pKa of Cys side-chain is 8.2, Cys residues are partially negatively charged at pH 7.4, hence decreasing the net positive charge of Pvfp-5-Tyr at this pH and above and weakening the adhesion with the negatively-charged mica surface. Furthermore, thiolates may also interact with other basic residues of Pvfp-5-Tyr, further exacerbating the aggregation at higher pH. A similar trend was also observed upon repeating the adhesion measurements in an asymmetric geometry, in which only one mica surface was coated with either Pvfp-5-Dopa or Pvfp-5-Tyr (Figures 2c and S6). It is worth mentioning that the Dopa residues in Pvfp-5-Dopa can undergo a two-electron oxidation at pH 7.4, forming Dopaquinone, whereas the Tyr groups are stable at the same pH[30].

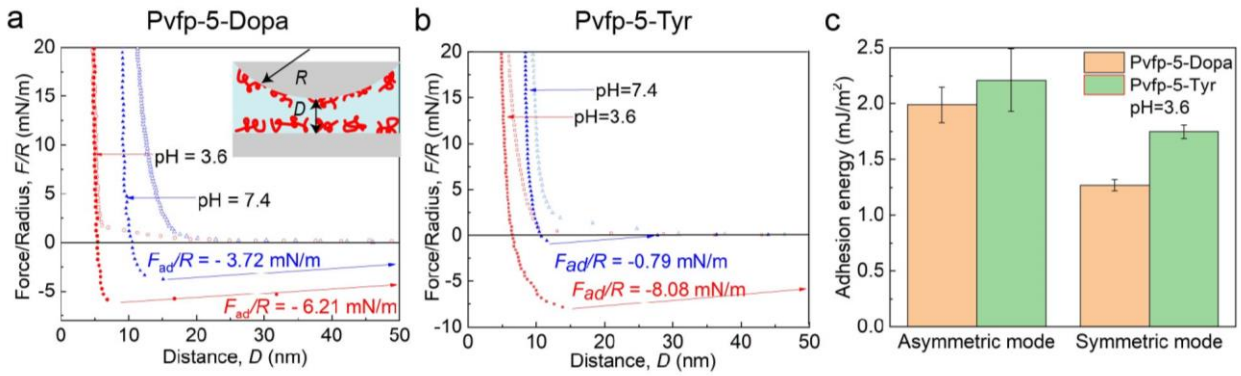

Figure 2. SFA adhesion measurements on Pvfp-5-Dopa and Pvfp-5-Tyr in the symmetric mode. **(a)** SFA force-distance profiles of Pvfp-5-Dopa at pH 3.6 and 7.4. Insert image is a schematic of the SFA measurements. **(b)** SFA force-distance profiles of Pvfp-5-Tyr at pH 3.6 and 7.4. **(c)** Adhesion energies of Pvfp-5-Dopa and Pvfp-5-Tyr measured by SFA in both symmetric and asymmetric modes.

The similar adhesive energies of Pvfp-5-Tyr and Pvfp-5-Dopa measured by the SFA indicates that converting Tyr to Dopa had little effect on adhesive properties of Pvfp-5. This is quite different from the properties of Mfp-5, the primer protein purified from *Mytilus californianus*, in which the Dopa residues play critical roles in the adhesive properties[31]. It has been suggested by MD simulations[12] that adhesion of Pvfp-5 is largely due to dipeptide of Tyr or Dopa with basic residues (Lys or Arg), whereby the paired residues bind to negatively charged surfaces via electrostatic interactions. Our SFA measurements agree with the MD simulations very well. Additionally, the difference between the adhesive behaviors of Pvfp-5β and MFP-5 can be attributed to the differences in their secondary structures. MFP-5 is largely unstructured in solution, whereas Pvfp-5 contains β-sheets, with four disulfide bonds formed between Cys^{51}– Cys^{60}, Cys^{65}–Cys^{76}, Cys^{70}–Cys^{87}, and Cys^{89}–Cys^{98}[16, 25]. Such rigid structure might prohibit Dopa's capability of forming bidentate hydrogen bond on the mica surface, which requires a molecular proximity between the two hydroxyl groups of a Dopa residue and the mica surface.

2.3 Phase behaviors of Pvfp-5 variants

It was previously reported that a MFP-3 derived peptide with Dopa undergoes LLPS at different pHs and ionic strengths[32]. To evaluate the phase behavior of the Pvfp-5β variants, 1 mg/ml of Pvfp-5-Tyr or Pvfp-5-Dopa were dissolved in 10 mM acetic acid and mixed with different pH buffers and ionic strengths to attain a ratio of 1:9 (protein:buffer) and final protein concentration of 0.1 mg/ml. For Pvfp-5-Dopa, at pH 7.5 and in 1 M ionic strength the solutions immediately became cloudy (Supplementary Video 1, Supporting Information) and optical microscopy observations confirmed the formation of coacervate microdroplets (Figure 3a). Within the time scale tested, the coacervate microdroplets exhibited no further morphological transformation. Turbidity measurements showed that Pvfp-5-Dopa could phase separate and form coacervate across a broad range of pH under different ionic strengths. At 0.1 M ionic strength, Pvfp-5-Dopa solution was transparent at pH 3. The turbidity of the solution slowly increased as we gradually raised the solution pH from 3 to 6.5 and then rapidly increased between pH 7 and 8.5, indicating that the coacervates are more easily formed near neutral pH. A similar trend was observed in solutions with 0.5 M and 1 M ionic strength, with higher ionic strength leading to a more turbid solution at the same pH (Figure 3b). In stark contrast, Pvfp-5-Tyr only exhibited slight increase of turbidity with the increase of pH and ionic strength, and optical microscopy observations showed that only irregular aggregates were formed (Figure 3c and S7).

To further explore the LLPS conditions of Pvfp-5-Dopa, we established the phase diagram of Pvfp-5-Dopa as a function of protein concentration and solution ionic strength at pH 8.2. Pvfp-5-Dopa could form coacervate microdroplets with a minimum protein concentration of 0.05 $mg.mL^{-1}$ and a NaCl concentration of 0.3 M (Figure 3d). Increasing the NaCl concentration of the solution resulted in larger microdroplets due to a stronger electrostatic screening, which decreases the electrostatic repulsion between the Pvfp-5-

Dopa coacervate microdroplets and promotes their coalescence[33]. To enhance the visualization of Pvfp-5-Dopa microdroplets, we added 0.1 mg of green fluorescent protein (GFP) to the 90 μL of buffer solution (pH 7.5 with 1 M NaCl) and mixed with 10 μL of 1 mg mL^{-1} of Pvfp-5-Dopa to reach a final concentration of 0.1 mg mL^{-1} to induce phase separation. The microdroplets exhibited a strong green fluorescent signal (Figure 3e), further confirming that the incorporation of Dopa to Pvfp-5 led to LLPS, with a capability to recruit client molecules such as GFP.

2.4 Adsorption and adhesive behaviour of Pvfp-5 variants

The adhesive properties of the Pvfp-5 variants were investigated by Quartz Crystal Microbalance (QCM) measurements on titanium dioxide (TiO_2) surfaces in acetic acid buffer (pH 3.5) for the soluble proteins or in PBS buffer for Pvfp-5-Dopa coacervates. The resonance frequency change is directly correlated to mass adsorption on the surfaces. After buffer flushing, Pvfp-5-Tyr (Δf_{ads} = 6.8 Hz) and Pvfp-5-Dopa (Δf_{ads} = 12.3) showed moderate adsorption on the TiO_2 surface. Upon phase separation, Pvfp-5-Dopa coacervate microdroplets displayed a much stronger adsorption on TiO_2 surfaces (Δf_{ads} = 23.8 Hz) (Figure 3f), indicating that in the coacervate state, Pvfp-5-Dopa has a stronger binding to TiO_2 surfaces compared to its solution state.

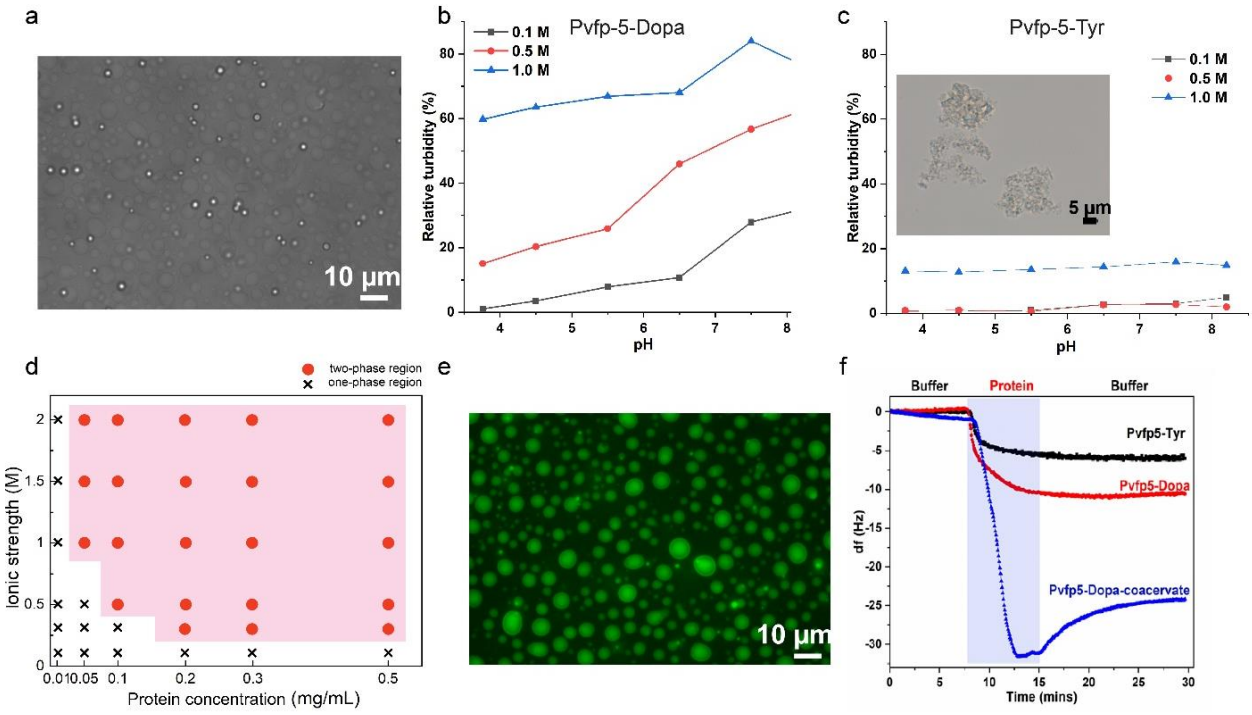

Figure 3. Phase behaviors of Pvfp-5 variants**. (a)** Light microscopy image of Pvfp-5-Dopa coacervates at pH 8.2 and 1 M ionic strength. **(b,c)** Relative turbidity of Pvfp-5-Dopa (b) and Pvfp-5-Tyr (c) *vs.* pH at different ionic strengths. Inlet in (c) is an optical micrograph of Pvfp-5-Tyr aggregates at pH 7.5, 1 M ionic strength. **(d)** Phase diagram of Pvfp-5-Dopa at different protein concentration and ionic strength. **(e)** Fluorescence micrograph of Pvfp-5-Dopa coacervate loaded with green fluorescent protein at pH 7.5, 1 M ionic strength. **(f)** QCM plots for the adsorption of Pvfp-5-Tyr, Pvfp-5-Dopa, and Pvfp-5-Dopa coacervates on titanium dioxide surfaces.

The adhesive properties of the Pvfp-5-Dopa coacervates were also investigated by SFA. 20 μL of Pvfp-5-Dopa in PBS buffer (I = 1M) was injected in between of two mica surfaces and equilibrated for 30 min before the measurement. The SFA force-distance profiles corroborated that Pvfp-5-Dopa coacervate microdroplets exhibit liquid-like properties. The coacervates coated on both mica surfaces coalesced into a single film of 25 nm when bringing the two surfaces into contact. There was no long-range repulsion measured beyond the distance of 40 nm. Upon separation, a viscous capillary formed between the surfaces, resulting in an adhesion force (Figure 4a), which is mainly caused by the interfacial tension

of the Pvfp-5-Dopa coacervate in solution. The effective interfacial tension can be calculated by:

$$\gamma_{eff} = F_{ad}/4\pi R \quad (2)$$

The interfacial tension of the Pvfp-5-Dopa coacervate calculated by Equation (2) is 0.63 ± 0.08 mJ/m^2, which is close to the interfacial tension of other self-coacervates formed by other mussel adhesive proteins[22, 34]. In comparison, Pvfp-5-Tyr formed solid aggregates under the same solution conditions, as evidenced by the SFA force-distance profiles, which revealed a long-range repulsion starting at around 450 nm distance (Figure 4b). The repulsion increased exponentially as the two surfaces were further compressed and there was no adhesion force measured during the separation, indicating that the two Pvfp-5-Tyr layers did not coalesce even under strong compression. Overall, the SFA measurements show that although converting Tyr to Dopa did not significantly change the adhesive property of Pvfp5 in the solution state (Figure 2), this conversion dramatically altered the phase behaviour and mechanical properties of Pvfp-5 structures that are obtained after pH increase: for Pvfp-5-Dopa, SFA curves with forces in the adhesion regime were characteristic of a viscous fluid formed by the coalescence of microdroplets, whereas for Pvfp-5-Tyr the absence of adhesion forces and presence of a thick repulsive wall were consistent with solid aggregates.

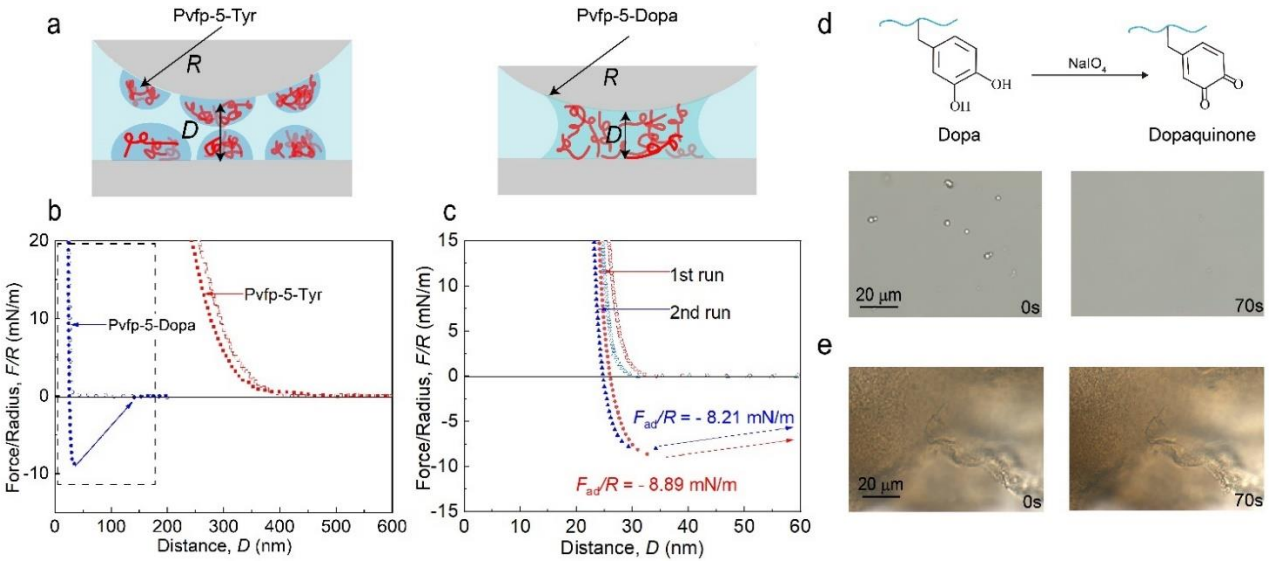

Figure 4. (a) Left: schematic of SFA measurements on Pvfp-5-Tyr. Right: Schematic of SFA measurements on Pvfp-5-Dopa. **(b)** Force distance profiles of Pvfp-5-Tyr aggregates and Pvfp-5-Dopa coacervates (20 μL of 0.1 mg·mL^{-1}) at pH 8.2 in PBS (I = 1M). **(c)** Zoom-in of force distance profiles of Pvfp-5-Dopa coacervates (20 μL of 0.1 mg·mL^{-1}) at pH 8.2 in PBS (I = 1M). **(d)** Upper: Sodium periodate oxidizes Dopa into Dopaquinone. Bottom: Pvfp-5-Dopa coacervates gradually disappeared after the addition of 1 μL 1M sodium periodate. **(e)** Pvfp-5-Tyr aggregates remained after the addition of 1 μL of 1 M sodium periodate.

We also performed controlled Dopa oxidation experiments to confirm the importance of Dopa in the coacervates of Pvfp-5-Dopa. Sodium periodate was used to oxidize Dopa into Dopaquinone[28]. After adding 1 μL of 1 M sodium periodate into 20 μL Pvfp-5-Dopa coacervates, the droplets disappeared in the solution within a few seconds. (Figure 4d, Supplementary Video 2). In comparison, Pvfp-5-Tyr aggregates under the same condition remained unchanged (Figure 4e, Supplementary Video 3). After Dopa oxidation, Dopaquinone loses the ability to forming bidentate H-bonds, which is critical to the coacervation of Pvfp-5-Dopa as discussed in the next Section. On the other hand, Pvfp-5-Tyr aggregates remain stable under the same chemical environment as sodium periodate cannot oxidize Tyr residues in solution. Periodate can also oxidize disulfide bonds into thiosulfonic esters, as well as cysteine into disulfides and sultines. However, periodate is unlikely to completely cleave the disulfide bonds between Cys residues.[35]

2.5 NMR studies and quantum chemistry (QC) calculations

To understand why the Tyr→Dopa substitution had such a strong effect on the phase behaviour of Pvfp-5β, we conducted solution NMR spectroscopy measurements of both proteins in order to identify the molecular level interactions that may regulate LLPS. The chemical structures of DOPA and Tyr with aromatic carbons according to NMR acronyms are shown in Figures 5a-b. HMQC (short and long range) spectra of free DOPA were obtained at the same pH conditions as Pvfp-5-Dopa and the assigned resonances were used as guidelines for interpretation of Pvfp-5-Dopa spectra (Figures S8a-d, Supporting Information). At pH 3.5, Pvfp-5-Dopa was in the soluble unfolded state and the resonances of $^{13}C\delta_2$, $^{13}C\varepsilon_2$, $^{13}C\gamma$, $^{13}C\varepsilon_1$ as well as $^{1}H\delta_2$ and $^{1}H\varepsilon_1$ was assigned unambiguously (Figure 5a, red). As the pH increased to 7.5, there was line broadening of $^{13}C\varepsilon_1/^{1}H\varepsilon_1$ and $^{13}C\varepsilon_2/^{1}H\delta_2$ (indicated with black arrows in Figure 5a), a phenomenon that can be attributed to the formation of interchain transient hydrogen bonding network involving both hydroxyl groups of Dopa at $^{13}C\zeta$ and $^{13}C\varepsilon_2$. This is highly reminiscent of Gln-Gln bonding network in FUS LC LLPS[36]. However, at pH 9.5 the cross-peaks assigned to $^{13}C\varepsilon_2/^{1}H\delta_2$ and $^{13}C\zeta/^{1}H\delta_2$ (Figure 5a, green) was again observed, owing to disassembly of coacervate microdroplets and subsequent aggregation of the Pvfp-5-Dopa (Figure S9), as also evidenced by optical microscopy observations. The absence, or line broadening, of the $^{13}C\zeta$ peak at pH 3.5 hints at the formation of nuclei of microdroplets that are too small to be observed by optical microscopy.

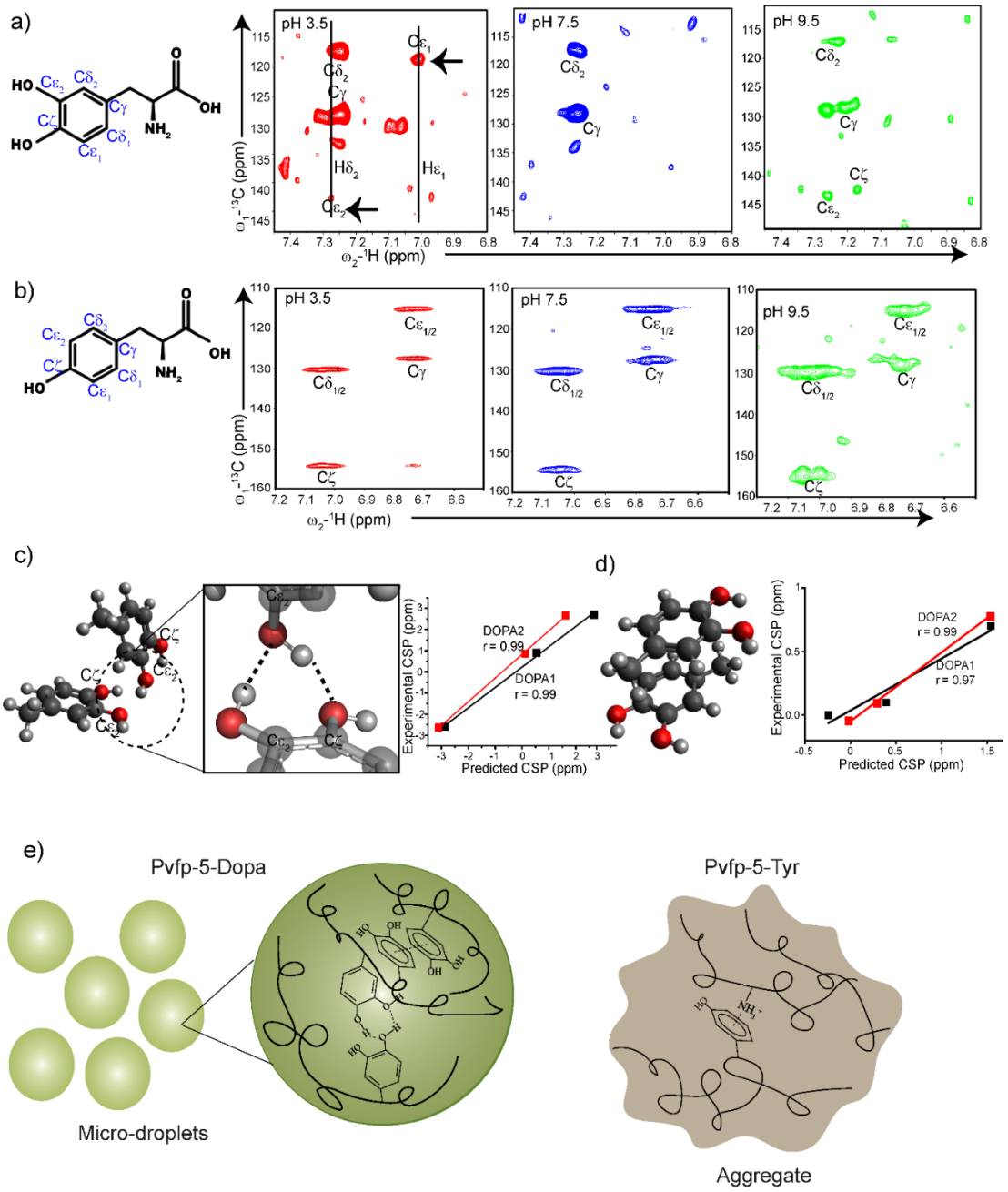

Figure 5. Natural abundance ^{13}C HMQC NMR studies of Pvfp-5-Dopa and Pvfp-5-Tyr. (a) ^{13}C HMQC long range (3-bond) spectra of 6 mg·mL^{-1} Pvfp-5-Dopa at pH 3.5 (red), 7.5 (blue) and 9.5 (green). The chemical structure of the Dopa molecule with aromatic carbon ring assigned according to NMR acronyms is shown on top. **(b)** ^{13}C HMQC long range (3-bond) spectra of 6 mg·mL^{-1}Pvfp-5-Tyr at pH 3.5 (red), 7.5 (blue) and 9.5 (green). The chemical structure of Tyr molecule with aromatic carbon ring assigned according to NMR acronyms is shown on top. **(c,d)** Experimental and calculated ^{13}C chemical shift perturbations (CSPs) of Pvfp-5-Dopa between pH 3.5 and 9.5 for bidentate hydrogen bonding (c) and π-π stacking of Dopa-Dopa (d) interactions. CSPs were calculated using the Quantum Chemical program GAUSSIAN (see Methods for details). **(e)** Schematic representation of the main intermolecular interactions in Pvfp-5-Dopa micro-droplets (left) and Pvfp-5-Tyr aggregates (right) identified by correlating quantum chemistry calculations with experimental ^{13}C CSPs.

The HMQC (short and long range) spectra of Pvfp-5-Tyr were also acquired at the same pH conditions as Pvfp-5-Dopa. In stark contrast, peak broadening was not observed and the resonances of the aromatic ring were present at all pHs (Figure 5b). At pH as high as 9.5, the protein aggregated, which was accompanied with splitting of resonances (Figure 5b, green). The corresponding chemical shift plot is shown in Figure S9 (Supporting Information).

Based on these chemical shift perturbations (CSPs), six different bonding configurations of Dopa and Tyr side-chains were computed using QC calculations, namely: *(i)* Lys-Tyr (cation-π) interaction; *(ii)* Tyr-Tyr (π-π) stacking; *(iii)* Lys-Dopa (cation-π) interaction; *(iv)* Dopa-Dopa H-bonding mediated by hydroxyl groups; *(v)* Dopa-Dopa (π-π) stacking; and *(vi)* Dopa-Dopa (π-π) stacking after oxidation of Dopa to dopaquinone at higher pH. Several reports have previously suggested a plausible cation-π interaction between Lys-Tyr residues in MFPs[14, 37-38]. QC calculations corroborated these observations, with a Pearson correlation *r* value of -0.99 when experimental *vs.* predicted chemical shift values of Pvfp-5-Tyr variants were plotted (Figure S10a, Supporting Information). π-π interactions of Tyr rings *(ii)* and Lys-Dopa cation-π *(iii)* were not supported in any of the configurations, with *r* values of 0.5 and -0.5, respectively (Figures S10b-c, Supporting Information). On the other hand, Dopa-Dopa H-bonding involving the aromatic hydroxyl groups (Figure 5c) and Dopa-Dopa (π-π) stacking (Figure 5d) was both favoured as indicated by a very good match between experimental and calculated CSPs. Dopa associated bidentate hydrogen bonding has previously been proposed for MFPs-derived peptides and peptoids[28, 39]. Our data indicate that this H-bonding network configuration, whereby the two hydroxyl groups of one Dopa residue interact with one hydroxyl group positioned on $C\varepsilon_2$ of a second Dopa residue (Figure 5c) might be one of the dominant molecular configurations mediating sticker-to-sticker (attractive) interactions during LLPS of Pvfp-5-Dopa. In contrast, this stabilizing triangular

configuration is not possible for Tyr because one -OH group is not sufficient to create this tripartite H-bonding network. In addition, our results indicate that Dopa-Dopa (but not Tyr-Tyr or Tyr-Dopa) π-π stacking configuration may also contribute to attractive interactions between stickers. Based on the available NMR data, we cannot distinguish the relative contributions of these two Dopa-Dopa configurations in the inter-sticker attraction. However, it should be noted that if bidental H-bond is the dominant configuration enabling LLPS in Pvfp-5-Dopa, it might protect Dopa oxidation under mildly alkaline pH conditions. However, above a critical pH of *ca.* 9.5, oxidation of Dopa occurs, thus abolishing the H-bonding network within the coacervate microdroplets and eventually resulting in disassembly of the coacervate microdroplets as observed by optical microscopy (Figure 4d).

3. Conclusion

In summary, in this study we have shown that Pvfp-5β exhibits LLPS under physiological conditions only when the Tyr residues are substituted to Dopa, resulting in the formation of coacervate microdroplets with high adsorption on solid surfaces and very low interfacial tension as measured by the SFA. Combining QC simulations with solution NMR spectroscopy, we find that LLPS of Pvfp-5-Dopa is enabled by inter-molecular interactions consisting of a specific triangular-shaped H-bonding network requiring two hydroxyl groups of the Dopa side-chain, as well as Dopa-Dopa π-π stacking. Neither of these intermolecular interactions are favored in Pvfp-5-Tyr, which instead forms aggregates that are predicted to be stabilized by intermolecular π-cation interactions. Our study thus suggests an important role for Dopa in MFPs beyond enhancing wet adhesion, namely regulation of LLPS as a way to concentrate the building blocks of adhesive plaques during their underwater fabrication. More generally, these findings suggest that the ability of certain proteins to exhibit LLPS

may be finely regulated by post-translational modifications that enable transient (H-bonding) attractive interactions, which favors the formation of a concentrated liquid phase as opposed to solid aggregates as schematically illustrated in Figure 5e.

4. Experimental Section

Cloning, Expression and Purification of Pvfp-5 Proteins. The gene encoding protein Pvfp-5 was constructed into pQE-80L. The above-mentioned construct was transformed into tyrosine auxotroph for the residue specific incorporation of Dopa. Then cells were grown in M9 minimal medium and expressed using 1mM Isopropyl β-d-1-thiogalactopyranoside. The Pvfp-5-Tyr and Pvfp-5-Dopa were purified using the same protocol as described earlier[10]. Purity and molecular weight of both proteins were analyzed by SDS-PAGE and Maldi-ToF mass spectrometry. Afterwards, the purified protein was freeze-dried and lyophilized. The NBT assay was used to confirm the successful incorporation of Dopa in place of Tyr into Pvfp-5 as described earlier[15]. Finally, both proteins were stored at -80 ˚C under argon atmosphere. During the whole protein purification, the samples were covered with an aluminum foil and kept on ice to prevent oxidation of Dopa.

Circular Dichroism. CD spectra were recorded to measure the secondary structures of Pvfp-5-Tyr and Pvfp-5-Dopa by using a Chirascan spectropolarimeter (Model 420, AVIV Biomedical Inc.). Pvfp-5 and Pvfp-5-Dopa were prepared at concentrations of 5 mg mL^{-1} in 10 mM acetic acid. Measurements were conducted in triplicates at wavelengths ranging from 190 to 260 nm, with 1 nm step size and 1 nm bandwidth at room temperature. The spectra were smoothed by the Savitzky–Golay method with a second-order polynomial[16].

Amino Acid Analysis. To determine the ratio of Tyr to Dopa and thereby to quantify the incorporation of Dopa during protein expression, a Ninhydrin-based amino acid analyzer

was used (Sykam, Eresing, Germany). Proteins samples were hydrolyzed in 200 µL of 6 M HCl solution and 10 µL 100% phenol in vacuum at 158 ˚C for 40 min. Afterwards washed with water and methanol, the hydrolyzed protein sample were finally dissolved in 0.2 M HCl and injected into the amino acid analyzer[16].

Turbidimetry for coacervation studies. 1 mg of Pvfp-5-Tyr and Pvfp-5-Dopa were dissolved in 10 mM acetic acid. Coacervate was formed by adding 10 µL of protein solution (1 mg) to 90 µL of PBS buffer to attain final protein concentration of 0.1 mg (volume ratio 1:9). Further, coacervation studies were performed at different pH (3.5 to 10) and different ionic strength (0.1 to 1.0 M) and different concentration of protein was then measured at 600 nm by UV-vis spectrophotometry (PerkinElmer Inc., Massachusetts, USA). Relative turbidity was calculated as earlier described[32, 40]. The coacervates droplets were visually inspected by inverted microscope with 63X oil immersion lens using a Zeiss “Axio observer z1” model (Carl Zeiss Pte Ltd, Oberkochen, Germany). Images were processed with AxioVision software. For fluorescence imaging, 1 mg mL^{-1} of Pvfp-5-Dopa was used to encapsulate 0.1 mg mL^{-1} of green fluorescent protein (GFP).

Optical Light Microscope. Light microscopy images were recorded using OLYMPUS IX73 Inverted Microscope. 20 µL of samples was dropped on a glass slide. Samples were then visualized at a magnification of 60×. Images analysis was done using the software of Lumenera corporation, Release 6.5.

Quartz Crystal Microbalance (QCM). 5-MHz piezoelectric quartz crystals coated with titanium dioxide (TiO_2) were purchased from Q-Sense (Frölunda, Sweden) and treated according to the protocol suggested before use. QCM experiments were carried out in a Q-Sense E4 QCM (Q-Sense, Sweden) instrument with four-channel IPC pump (Ismatec SA, Switzerland). Three cleaned crystals were mounted in the micro-fluidic chambers of the

QCM. On attaining stable resonant frequencies, proteins were injected in the three different channels, respectively, at a constant flow rate of 50 mL min^{-1}. Pvfp-5-Tyr and Pvfp-5-Dopa were prepared in degassed 10 mM acetic acid at a concentration of 0.1 mg mL^{-1} [16, 41]. To prepare Pvfp-5-Dopa coacervates, 0.1 mg/ml Pvfp-5-Dopa was dissolved in PBS buffer (0.1 M with 0.75 M NaCl to reach a total ionic strength I = 1M, pH = 8.2). In these experiments, 250 µL of 0.1 mg mL^{-1} of Pvfp-5-Tyr, Pvfp-5-Dopa and Pvfp-5-Dopa-coacervates were introduced for 2 min at a flow rate of 0.1 mL min^{-1} (adsorption step) before washing with buffer to desorb weakly bound proteins (desorption step).

Surface Forces Apparatus. The adhesion of Pvfp-5-Dopa and Pvfp-5-Tyr on Mica surfaces was studied using a surface forces apparatus 2000 (SFA 2000) with a reported geometry[27]. 55 nm thick sliver layer was deposited on the back side of mica surfaces glued on the SFA disks. The distance D between two surfaces is measured with the fringes of equal chromatic order (FECO) technique. By applying the Derjaguin approximation, the normalized adhesion force F/R between the two cylindrical SFA surfaces is directly proportional to the surface energy between two flat surfaces with a simple relation of $E_{ad} = F_{ad}/2\pi R$.[27, 42] For the protein adhesion measurement, 20 µL of 20 µg/ml Pvfp-5-Dopa and Pvfp-5-Tyr solution dissolved in acetate buffer (0.1M, pH = 3.6) was injected in between of two mica surfaces for the symmetric mode, and on one mica surface for the asymmetric mode. Buffer change was achieved by flushing the surfaces with 1mL 0.1M PBS (pH = 7.4). For measurements on coacervates, 0.1 mg/ml Pvfp-5-Dopa was dissolved in PBS buffer (0.1 M with 0.75 M NaCl to make the total ionic strength I = 1M; pH = 8.2) buffer to form coacervates. We refer to this buffer as PBS (I = 1 M) in the text. 20 µL of the coacervate solution was then injected in between of two mica surfaces. The system was equilibrated for 30 min before acquiring the force measurements. Milli-Q water (Smart2Pure™ Pro system, ThermoFisher) was used for all glassware cleaning and solution preparation.

Solution state NMR spectroscopy. All of the NMR experiments were carried out in Bruker 700 MHz spectrometer equipped with cryoprobe. Pvfp-5-Tyr and Pvfp-5-DOPA were dissolved in 10 mM acetic acid, pH 3.5 with D_2O (10%) and DSS (0.1 mM) for lock and internal reference respectively. ^{1}H NMR spectra of both the proteins were acquired with a spectral width of 16 ppm. 2D ^{1}H-^{15}N HSQC spectra of Pvfp-5-Tyr was acquired with 10 $mgmL^{-1}$ dissolved in 10 mM acetic acid, pH 3.5. 2D ^{1}H-^{1}H NOESY and 2D ^{1}H-^{1}H TOCSY spectra of Pvfp-5-Tyr were also acquired at sample conditions with 200 ms and 80 ms mixing time respectively. Natural abundance-2D ^{1}H-^{13}C HMQC short range (1-bond) and long range (3-bond) spectra were acquired with 64 and 128 scans respectively for pH 3.5, 5.5, 6.5, 7.5, 8.5 and 9.5. Aliquots from stock of 0.5 M NaOH was added to NMR samples for pH adjustments.

Quantum chemistry calculations. Quantum chemistry calculations were computed using Gaussian09 [36]. The predicted 13C chemical shit differences were obtained from the Gaussian quantum chemistry package. The experimental 13C chemical shift differences were obtained from pH titrations of Pvfp-5-Tyr and DOPA variants. Structural geometric optimizations were computed using the basis set wB97XD/cc-pVDZ. This basis set was chosen for its reasonable computational costs and acceptable precision of the 13C chemical shift predictions. All optimized structures were subjected to further refinement using the Gauge-Independent Atomic Orbital (GIAO) method. Spin-spin coupling constants were also computed. No scaling was performed as chemical shift differences were computed and reported in text for comparison to the chemical shift differences obtained from the experimental data. Computed values were fitted to the experimental data to assess the accuracy of the calculations performed. Input files of the side chain of the residues were prepared using a molecular editor, Avogadro 1.2.0. Output structures were examined using the same molecular editor.

Acknowledgements

This work was supported by the Singapore Ministry of Education (MOE) through an Academic Research Fund (AcRF) Tier 3 grant (# MOE 2019-T3-1-012). Q. G and J. Y acknowledge funding from the Singapore National Research Fellowship (NRF-NRFF11-2019-0004).

References

[1] B. P. Lee, P. B. Messersmith, J. N. Israelachvili, J. H. Waite, *Annu. Rev. Mater. Res.* **2011**, 41, 99.
[2] H. Lee, N. F. Scherer, P. B. Messersmith, *Proc. Natl. Acad. Sci.* **2006**, 103, 12999.
[3] J. H. Waite, *J. Exp. Biol.* **2017**, 220, 517.
[4] Q. Guo, J. Chen, J. Wang, H. Zeng, J. Yu, *Nanoscale* **2020**, 12, 1307.
[5] M. J. Harrington, A. Masic, N. Holten-Andersen, J. H. Waite, P. Fratzl, *Science* **2010**, 328, 216.
[6] T. H. Anderson, J. Yu, A. Estrada, M. U. Hammer, J. H. Waite, J. N. Israelachvili, *Adv. Funct. Mater.* **2010**, 20, 4196.
[7] W. Wei, J. Yu, C. Broomell, J. N. Israelachvili, J. H. Waite, *J. Am. Chem. Soc.* **2013**, 135, 377.
[8] P. Kord Forooshani, B. P. Lee, *J. Polym. Sci., Part A: Polym. Chem.* **2017**, 55, 9.
[9] J. H. Ryu, P. B. Messersmith, H. Lee, *ACS Appl. Mater. Interfaces* **2018**, 10, 7523.
[10] P. Bilotto, C. Labate, M. P. De Santo, K. Deepankumar, A. Miserez, B. Zappone, *Langmuir* **2019**, 35, 15481.
[11] P. A. Guerette, S. Hoon, Y. Seow, M. Raida, A. Masic, F. T. Wong, V. H. B. Ho, K. W. Kong, M. C. Demirel, A. Pena-Francesch, S. Amini, G. Z. Tay, D. Ding, A. Miserez, *Nat. Biotechnol.* **2013**, 31, 908.
[12] X. Ou, B. Xue, Y. Lao, Y. Wutthinitikornkit, R. Tian, A. Zou, L. Yang, W. Wang, Y. Cao, J. Li, *Sci. Adv.* **2020**, 6, eabb7620.
[13] G. P. Maier, M. V. Rapp, J. H. Waite, J. N. Israelachvili, A. Butler, *Science* **2015**, 349, 628.
[14] M. A. Gebbie, W. Wei, A. M. Schrader, T. R. Cristiani, H. A. Dobbs, M. Idso, B. F. Chmelka, J. H. Waite, J. N. Israelachvili, *Nat. Chem.* **2017**, 9, 473.
[15] K. Deepankumar, C. Lim, I. Polte, B. Zappone, C. Labate, M. P. De Santo, H. Mohanram, A. Palaniappan, D. S. Hwang, A. Miserez, *Adv. Funct. Mater.* **2020**, 30, 1907534.
[16] L. Petrone, A. Kumar, C. N. Sutanto, N. J. Patil, S. Kannan, A. Palaniappan, S. Amini, B. Zappone, C. Verma, A. Miserez, *Nat. Commun.* **2015**, 6, 8737.
[17] S. Amini, S. Kolle, L. Petrone, O. Ahanotu, S. Sunny, C. N. Sutanto, S. Hoon, L. Cohen, J. C. Weaver, J. Aizenberg, N. Vogel, A. Miserez, *Science* **2017**, 357, 668.
[18] M. Cui, X. Wang, B. An, C. Zhang, X. Gui, K. Li, Y. Li, P. Ge, J. Zhang, C. Liu, C. Zhong, *Sci. Adv.* **2019**, 5, eaax3155.
[19] T. Priemel, E. Degtyar, M. N. Dean, M. J. Harrington, *Nat. Commun.* **2017**, 8, 14539.
[20] E. Valois, R. Mirshafian, J. H. Waite, *Sci. Adv.* **2020**, 6, eaaz6486.
[21] T. Priemel, R. Palia, M. Babych, C. J. Thibodeaux, S. Bourgault, M. J. Harrington, *Proc. Natl. Acad. Sci.* **2020**, 117, 7613.
[22] W. Wei, Y. Tan, N. R. Martinez Rodriguez, J. Yu, J. N. Israelachvili, J. H. Waite, *Acta Biomater.* **2014**, 10, 1663.
[23] N. Ayyadurai, N. S. Prabhu, K. Deepankumar, Y. J. Jang, N. Chitrapriya, E. Song, N. Lee, S. K. Kim, B.-G. Kim, N. Soundrarajan, S. Lee, H. J. Cha, N. Budisa, H. Yun, *Bioconjugate Chem.* **2011**, 22, 551.
[24] P. Bilotto, M. Lengauer, J. Andersson, U. Ramach, L. L. E. Mears, M. Valtiner, *Langmuir* **2019**, 35, 15552.
[25] R. Santonocito, F. Venturella, F. Dal Piaz, M. A. Morando, A. Provenzano, E. Rao, M. A. Costa, D. Bulone, P. L. San Biagio, D. Giacomazza, A. Sicorello, C. Alfano, R. Passantino, A. Pastore, *J. Biol. Chem.* **2019**, 294, 12826.

[26] P. G. Vadakkedath, D. J. McGillivray, *J. Phys.: Conf. Ser.* **2020**, 1537, 012014.
[27] J. Israelachvili, Y. Min, M. Akbulut, A. Alig, G. Carver, W. Greene, K. Kristiansen, E. Meyer, N. Pesika, K. Rosenberg, H. Zeng, *Rep. Prog. Phys.* **2010**, 73, 036601.
[28] J. Yu, W. Wei, E. Danner, J. N. Israelachvili, J. H. Waite, *Adv. Mater.* **2011**, 23, 2362.
[29] Q. Lin, D. Gourdon, C. Sun, N. Holten-Andersen, T. H. Anderson, J. H. Waite, J. N. Israelachvili, *Proc. Natl. Acad. Sci.* **2007**, 104, 3782.
[30] W. Wei, J. Yu, M. A. Gebbie, Y. Tan, N. R. Martinez Rodriguez, J. N. Israelachvili, J. H. Waite, *Langmuir* **2015**, 31, 1105.
[31] E. W. Danner, Y. Kan, M. U. Hammer, J. N. Israelachvili, J. H. Waite, *Biochemistry* **2012**, 51, 6511.
[32] W. Wei, L. Petrone, Y. Tan, H. Cai, J. N. Israelachvili, A. Miserez, J. H. Waite, *Adv. Funct. Mater.* **2016**, 26, 3496.
[33] S. Meng, J. M. Ting, H. Wu, M. V. Tirrell, *Macromolecules* **2020**, 53, 7944.
[34] D. S. Hwang, H. Zeng, A. Srivastava, D. V. Krogstad, M. Tirrell, J. N. Israelachvili, J. H. Waite, *Soft Matter* **2010**, 6, 3232.
[35] A. Sudalai, A. Khenkin, R. Neumann, *Org. Biomol. Chem.* **2015**, 13, 4374.
[36] A. C. Murthy, G. L. Dignon, Y. Kan, G. H. Zerze, S. H. Parekh, J. Mittal, N. L. Fawzi, *Nat. Struct. Mol. Biol.* **2019**, 26, 637.
[37] S. Park, S. Kim, Y. Jho, D. S. Hwang, *Langmuir* **2019**, 35, 16002.
[38] S. Kim, A. Faghihnejad, Y. Lee, Y. Jho, H. Zeng, D. S. Hwang, *J. Mater. Chem. B* **2015**, 3, 738.
[39] W. R. Wonderly, T. R. Cristiani, K. C. Cunha, G. D. Degen, J.-E. Shea, J. H. Waite, *Macromolecules* **2020**, 53, 6767.
[40] Z. W. Lim, Y. Ping, A. Miserez, *Bioconjugate Chem.* **2018**, 29, 2176.
[41] K. Deepankumar, A. George, G. Krishna Priya, M. Ilamaran, N. R. Kamini, T. S. Senthil, S. Easwaramoorthi, N. Ayyadurai, *ACS Sustainable Chem. Eng.* **2017**, 5, 72.
[42] M. Valtiner, S. H. Donaldson, M. A. Gebbie, J. N. Israelachvili, *J. Am. Chem. Soc.* **2012**, 134, 1746.